Article

The Inhibition of H1N1 Influenza Virus-Induced Apoptosis by Surface Decoration of Selenium Nanoparticles with β-Thujaplicin through Reactive Oxygen Species-Mediated AKT and p53 Signaling Pathways

Changbing Wang, Haiyang Chen, Danyang Chen, Mingqi Zhao, Zhengfang Lin, Min Guo, Tiantian Xu, Yi Chen, Liang Hua, Tao Lin, Ying Tang, Bing Zhu,* and Yinghua Li*

Cite This: ACS Omega 2020, 5, 30633−30642

Read Online

ACCESS | Metrics & More | Article Recommendations

ABSTRACT: β-Thujaplicin possess a variety of biological activities. The use of modified biological nanoparticles (NPs) to develop novel anti-influenza drugs has increased in recent years. Selenium nanoparticles (SeNPs) with antiviral activity have attracted increasing attention for biomedical intervention. Functionalized SeNPs by β-thujaplicin (Se@TP) surface modified with superior antiviral activity were synthesized in this study. Compared to a virus group (43%), when treated with Se@TP (88%), the cell survival rate of MDCK cells was 45% higher. Se@TP could inhibit H1N1 from infecting Madin-Darby canine kidney (MDCK) cells and block chromatin condensation and DNA fragmentation. Se@TP obviously prevented MDCK cells from generating reactive oxygen species. Furthermore, Se@TP prevents lung injury in H1N1-infected mice through eosin staining and hematoxylin *in vivo*. Mechanistic investigation revealed that Se@TP inhibited H1N1 influenza virus from infecting MDCK cells through induction of apoptosis via suppressing AKT and p53 signaling pathways through immunohistochemical assay. Our results suggest that β-thujaplicin-modified SeNPs as carriers are an efficient way to achieve an antiviral pharmaceutical candidate for H1N1 influenza.
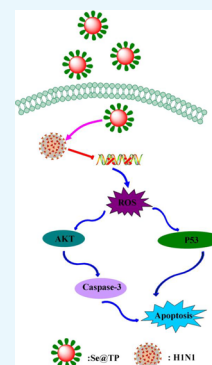
INTRODUCTION

As a segmented RNA virus, influenza virus affects millions of people and is still a serious contagious pathogen in seasonal epidemics.[1,2] H1N1 influenza virus is a highly infectious respiratory disease, which belongs to influenza A type viruses.[3] H1N1 influenza virus was discovered and identified in the U.S. and Mexico in 2009, which infected more than 8768 deaths in 207 countries.[4] Due to the arising mutation of antigenic shifts and the genome in different species, influenza virus may emerge a novel influenza among humans in the future.[5] The influenza infection cycle included three steps: first, the influenza viruses attach to the host cell surface receptor and fuse with the endosomal membrane. Second, uncoating of nucleocapsid and multiplication of the genetic material occurs. Finally, the influenza protein and new viron is expressed and released.[6,7] On the surface of influenza virus, there are two important glycoproteins: hemagglutinin (HA) and neuraminidase (NA).[8] In the early stage of viral infection, HA combined sialic acid-containing receptors on host cells and mediated the entry and fusion of virus.[9,10] When mature viruses separate from the host cell surface, NA plays an important role in assisting the virus cleave the linkage between sialic acid and hemagglutinin.[11] Although the conventional way to restrain the spread of influenza infections is vaccination, restraining the spread of influenza infections is a long period between the rapid virus evolution and vaccine development.[12]

β-Thujaplicin (2-hydroxy-4-isopropyl-2,4,6-cycloheptatrieneone) is an antimicrobial tropolone derived from geranyl pyrophosphate (GPP) and monoterpene intermediate.[13,14] β-Thujaplicin has been reported to possess antibacterial and antifungal activities.[15,16] However, the anti-influenza virus effects of β-thujaplicin remain unclear.[17,18] The nanotechnology provided a new prospect to solve these problems.[19,20] Also, the new antiviral nanodrug should effectively inhibit viral infection with fewer cytotoxicity.[21−23] Poor immunogenicity of M2e presents a significant roadblock, and gold nanoparticles conjugated to consensus M2e peptide against influenza A viruses was reported by Tao et al.[24] By gradually increasing the size of ligand-functionalized gold nanoparticles up to virus-like dimensions, different sizes of polyvalent nanoparticles used to inhibit virus was reported by Vonnemann et al.[25] Nanoparticles have been used to improve systemic immune response
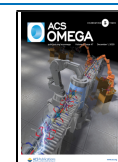
to infectious disease of virus, and Wang et al. reported that SiO_2@LDH nanoparticles enhance the response of hepatitis B virus DNA vaccine.[26] Self-assembly of viral coating proteins encapsulating functional nanoparticles provides a new class of biomaterials for potential application, and Shen et al. reported efficient encapsulation of Fe_3O_4 nanoparticles into genetically engineered hepatitis B core virus-like particles.[27] Silver nanoparticles have antiviral properties, and Zhang et al. reported that silver nanoparticle treatment ameliorates biliary atresia syndrome in rhesus rotavirus-inoculated mice.[28] Among them, selenium nanoparticles (SeNPs) attract much attention due to their unique antimicrobial activities.[29] Selenium is an integral component of several selenoproteins, which controls several crucial biological processes.[30−32] The deficiency of selenium could enhance the susceptibility to infections including respiratory virus infections.[33] Therefore, the aim of the present study was to expose novel-functionalized selenium nanoparticles, which can inhibit the infection of H1N1 virus. We hypothesized that β-thujaplicin-modified SeNPs (Se@TP) have excellent antiviral activity against H1N1 virus. Though several research groups have described the antimicrobial effects of SeNPs, the antiviral mechanisms are still unclear.[34,35] This study was to verify how β-thujaplicin-modified SeNPs inhibit H1N1 influenza virus *in vitro* and *in vivo*.

■ RESULTS AND DISCUSSION

Preparation and Characterization of Se@TP. The light images and Tyndall effect of Se@TP are as shown in Figure 1A−C, and the results indicated that Se@TP nanoparticles
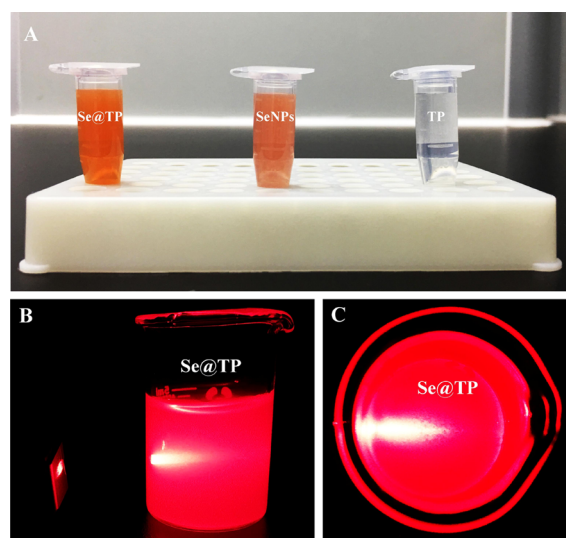

Figure 1. Ligc, SeNPs, and TP. (A) Color changes in Se@TP, SeNPs, and TP. (B,C) Tyndall effect in Se@TP.

were synthesized. The morphology of Se@TP presents spherical-shaped particles in Figure 2A. TP modified with SeNPs formed more compact and stable globular nanocomposites. As shown in Figure 2B, energy dispersive X-ray analysis (EDX) indicated signals of C (10%) and O (8%) from TP, and the percentage of Se atoms was 82%. As shown in (Figure 2C,D), Se@TP was decreased from 200 to 80 nm, which indicated much smaller size. The zeta potential of SeNPs (−25 mV) was lower than Se@TP (8 mV), demonstrating the higher stability of Se@TP than SeNPs.

Antiviral Activity of Se@TP. MDCK cells infected by H1N1 influenza showed a decrease in cell numbers and loss of cell-to-cell contact as shown in Figure 3A. When cotreated with Se@TP, the cell's morphology slightly changed. In Figure 3B, the cell viabilities were 26% (virus), 43% (virus + TP), 67% (virus + SeNPs) and 88% (virus + Se@TP). The results indicated that the antiviral activity of SeNPs was effectively amplified by TP. Minimum inhibitory concentration (MIC) of drug A combination present in Se@TP of Se (125 μM); MIC of drug B combination present in Se@TP of TP (2.5 μM); MIC of drug A alone corresponded to free SeNPs (1 mM); and MIC of drug B alone corresponded to free TP (10 μM). Fractional inhibitory concentration (FIC) was calculated as (MIC drug A combination/MIC drug A alone) + (MIC drug B combination/MIC drug B alone) =125 μM/1 mM + 2.5/10 μM = 0.375. FIC was 0.375, below 0.5, indicating synergy. In this study, the FIC index was basically interpreted as follows: FIC < 0.5, synergy; FIC between 0.5 and 2, indifference; FIC > 2, antagonism. The results suggest that Se@TP effectively inhibited the proliferation of H1N1 influenza virus.

Intracellular Localization of Se@TP. The lysosomes were found and increased in a time-dependent manner in MDCK cells as shown in Figure 4. After 30 min, Se@TP escaped from lysosomes and transported in the cytosol. Then, distributed into the cells after 60 min. This result showed that the target organelle of Se@TP was lysosome.

Depletion of Mitochondrial Membrane Potential (ΔΨm) and Translocation of Phosphatidylserine Induced by Se@TP. Treatments of MDCK cells with H1N1 influenza virus resulted in elevation of mitochondrial depolarization and dysfunction as shown in Figure 5A. Compared to TP and SeNPs, when MDCK cells were exposed to Se@TP, the percentage of mitochondrial membrane potential was significantly increased. These results demonstrate that Se@TP inhibited H1N1 influenza virus by apoptosis in MDCK cells through inducting mitochondrial dysfunction. As shown in Figure 5B, MDCK cells treated with Se@TP revealed a decrease in cell number. The results demonstrate that Se@TP restrained H1N1 virus infection of MDCK cells mainly through inhibiting apoptosis.

Inhibition of H1N1 Infection of MDCK Cells by Se@TP. Flow cytometry and TUNEL-DAPI were employed to examine the antivirus mechanisms of Se@TP. As shown in Figure 6A, the cell population of sub-G1 that represents apoptosis was significantly increased in the DNA histogram with H1N1 infection. However, compared to TP and SeNPs, Se@TP significantly decreased the apoptotic cell population to 30.4%. As shown in Figure 6B, MDCK cells exhibited typical apoptotic features with H1N1 influenza virus with DNA fragmentation and nuclear condensation. Cotreatment with Se@TP remarkably prevented the H1N1 influenza virus-induced changes in nuclear morphology. These results indicated that Se@TP rescues MDCK cells from H1N1 influenza virus-induced apoptosis.

Detection of Caspase-3 Activity. The caspase-3 activities were 451% (virus), 332% (virus + TP), 290% (virus + SeNPs), and 190% (virus + Se@TP) as shown in Figure 7. The treatment of H1N1 influenza virus-infected MDCK cells remarkably increased the activity. TP and SeNPs slightly inhibited the caspase-3 activity, and Se@TP significantly decreased the caspase-3 activity. The result showed that the Se@TP inhibits the H1N1 influenza virus through caspase-3 activity.
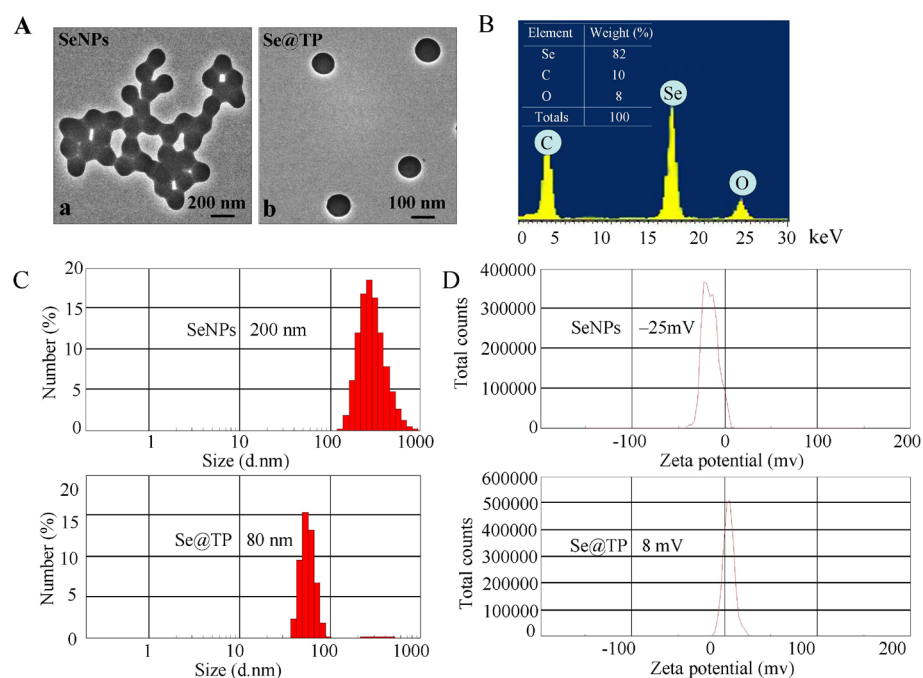
Figure 2. Characterization of SeNPs and Se@TP. (A) TEM images of SeNPs and Se@TP. (B) EDX analysis of Se@TP. (C) Size distribution of SeNPs and Se@TP. (D) Zeta potentials of SeNPs and Se@TP.
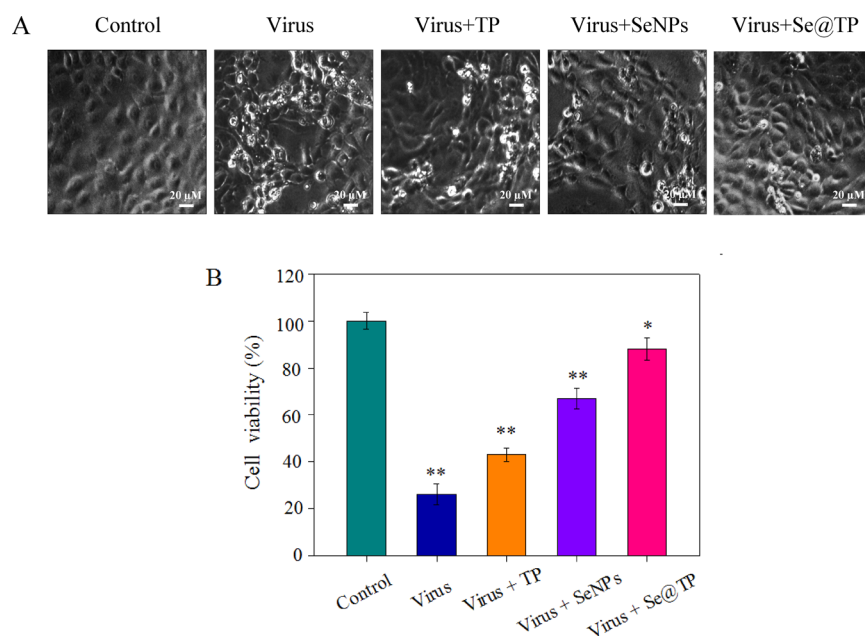

Figure 3. Effects of Se@TP on the growth of H1N1 infection of MDCK cells by MTT assay. (A) Morphological changes in H1N1-infected MDCK cells observed by phase contrast microscopy. (B) Antiviral activity of Se@TP. Concentration of SeNPs was 1 mM and TP 10 μM. Bars with different characters are statistically different at $*p < 0.05$ or $**p < 0.01$ level.

Inhibition of ROS Generation by Se@TP. The ROS generation was conducted by DCF determination to indicate the action mechanisms of Se@TP. The intracellular ROS generations were 430% (virus), 332% (virus + TP), 260% (virus + SeNPs) and 130% (virus + Se@TP) as shown in Figure 8A. TP and SeNPs slightly inhibited the ROS generation. However, Se@TP remarkably decreased the ratio of ROS generation. The fluorescence intensity of DCF treated with H1N1 influenza virus was much stronger than TP, SeNPs, and Se@TP in Figure 8B. Microvilli and mitochondria were observed in MCK cells. As shown in Figure 9A, when MDCK

cells were incubated with H1N1 influenza virus, the TEM image indicated distorted organelles, shrunken cytoplasm, and condensed chromatin. The mitochondria of MDCK cells recovered in shape after treatment with Se@TP in Figure 9B. The results indicate the ROS participated in the antiviral action.

ROS-Mediated Signaling Pathways by Se@TP. The overexpression of ROS could lead to DNA damage through regulation of apoptosis signaling pathways. As shown in Figure 10, compared to TP and SeNPs, treatments of the cells with Se@TP obviously inhibited the expression levels of phos-
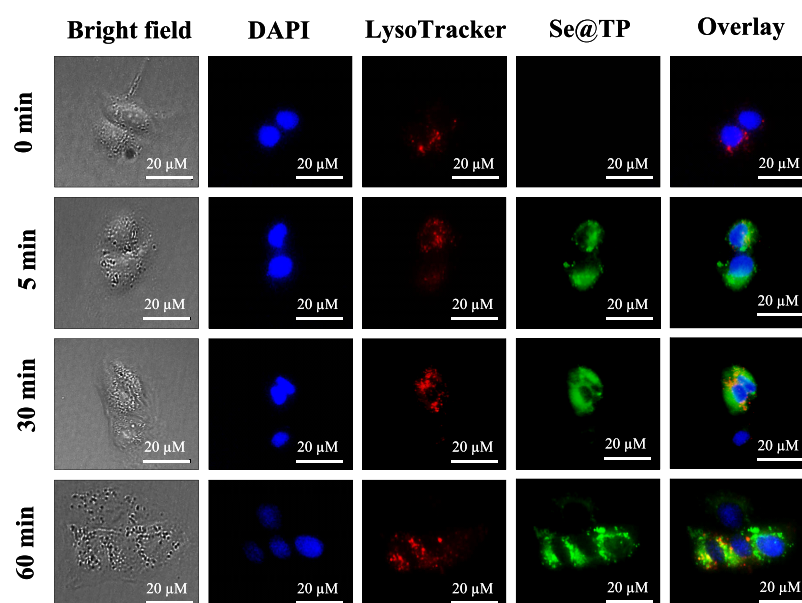
Figure 4. Localization of coumarin-6-loaded Se@TP in MDCK cells. The cells were treated with coumarin-6-loaded Se@TP for different periods of time and were observed under a fluorescence microscope stained with LysoTracker (red fluorescence, lysosome) and DAPI (blue fluorescence, nucleus)
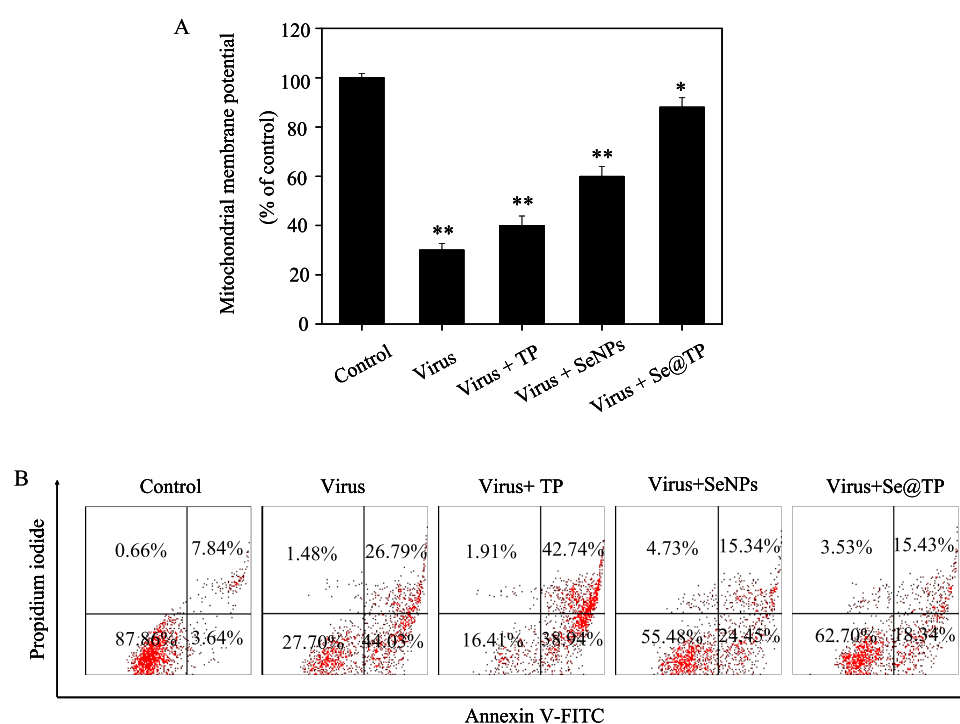

Figure 5. Depletion of mitochondrial membrane potential and translocation of phosphatidylserine induced by SeNPs, TP, and Se@TP. (A) Mitochondrial membrane potential of H1N1 infection of MDCK cells exposed to SeNPs, TP, and Se@TP. (B) Translocation of phosphatidylserine induced by SeNPs, TP, and Se@TP in H1N1 infection of MDCK cells.

phorylated and total AKT in MDCK cells. Similarly, for the p53 signaling pathway, Se@TP significantly increased the levels of p-p53 protein and total of p53. These results reveal that Se@OTV inhibited H1N1 influenza virus-induced MDCK cells apoptosis by ROS-mediated AKT and p53 signaling pathways.

***In Vivo* Antiviral Activity.** Mice were infected with H1N1 virus and treated with TP, SeNPs, and Se@TP, followed by HE staining, TUNEL analyses, and immunohistochemical test

of lung tissues after being executed. As the HE staining presents (Figure 11), the H1N1-infected group was manifested as alveolar collapse, perivascular, and peribronchiolar edema. When treated with TP or SeNPs, the symptoms lessened. Se@TP attenuated the histopathological manifestations substantially. The result indicated that Se@TP protected the lungs from being injured. Se@TP nanoparticles prevented the DNA damage during H1N1 infection. Meanwhile, the HE staining and TUNEL analysis illustrated that Se@TP inhibited MDCK
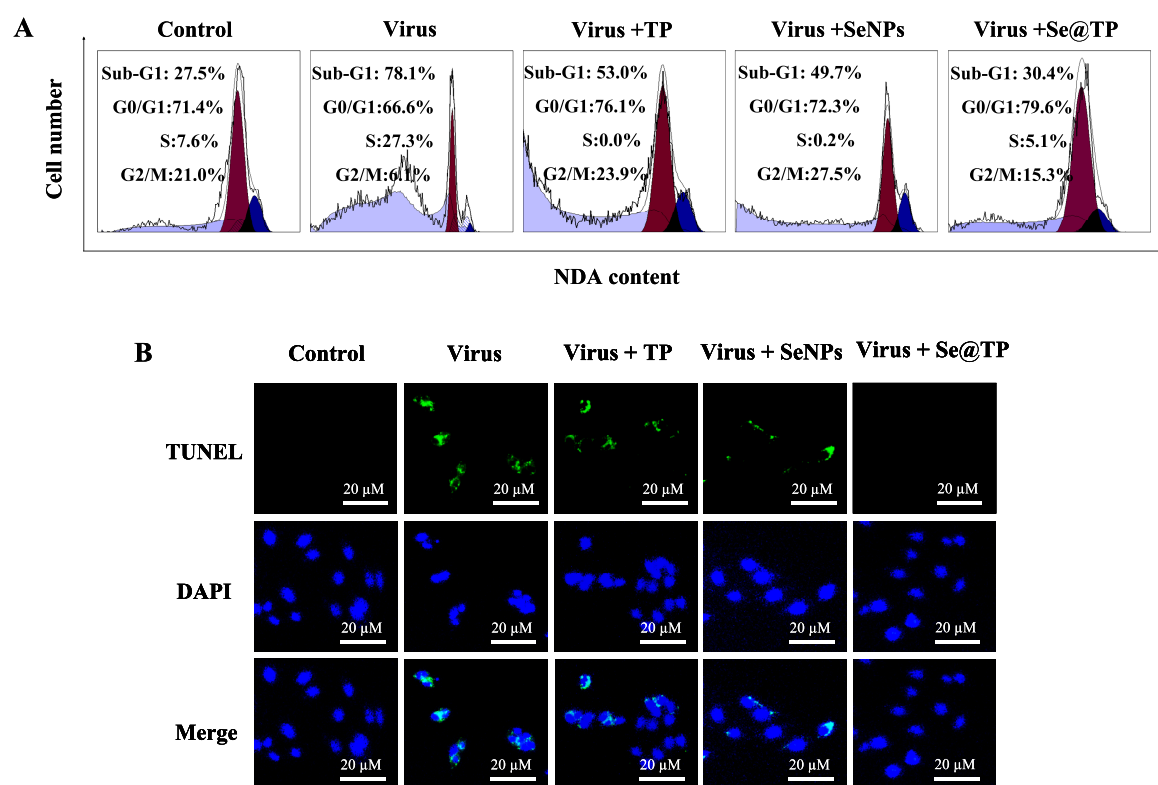
Figure 6. Se@TP-induced apoptosis in H1N1 infection of MDCK cells. (A) Cell cycle distribution after different treatments was analyzed by quantifying DNA content using flow cytometric analysis. (B) DNA fragmentation and nuclear condensation as detected by TUNEL-DAPI costaining assay. All results were representative of three independent experiments.
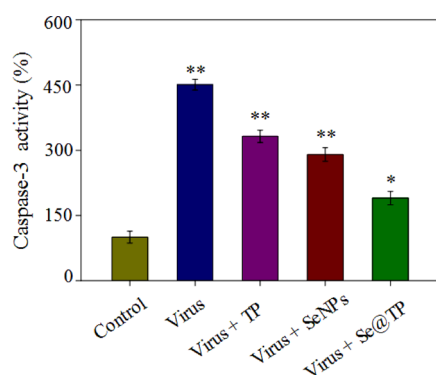

Figure 7. Inhibition of caspase-3 activity by Se@TP. Cells were treated with TP, SeNPs, Se@TP, and caspase-3 activity and were detected by a synthetic fluorogenic substrate. Concentration of SeNPs was 1 mM and TP 10 μM. Bars with different characters are statistically different at *$p < 0.05$ or **$p < 0.01$ level.

cell infection by H1N1 influenza virus. Caspase-3, P-AKT, T-AKT, p-p53, and p53 proteins were detected and positive after H1N1 virus infection as shown in Figure 12. The lung index was a reliable indicator of lung lesion levels. Lung index of mice was calculated for each group (Figure 13): control (0.59), virus (1.66), virus + TP (1.34), virus + SeNPs (1.17), and virus + Se@TP (0.89). The survival analysis and the change in the body of influenza virus-infected BALB/c mice and treated with Se@TP are shown in Figure 14A,B. The mice in the H1N1 influenza group showed severe weight loss. When treated with Se@TP, the percent survival was higher than TP and SeNPs. The results demonstrated that Se@TP protected the mice from H1N1 influenza infection. The scheme of H1N1

influenza virus-induced MDCK cell apoptosis by ROS-mediated AKT and p53 signaling pathway are shown in Figure 15.

CONCLUSIONS

In conclusion, Se@TP with lower toxicity exhibits superior antiviral abilities to prevent H1N1 influenza virus infection in this study. The mechanisms of antiviral activity showed that Se@TP inhibited caspase-3-mediated apoptosis through ROS generation. *In vivo* antiviral result showed that Se@TP inhibited MDCK cells apoptosis through regulating the AKT and p53 signaling pathways. In summary, the nanosystem of Se@TP might provide a promising selenium species with antiviral activity against H1N1 influenza virus.

MATERIALS AND METHODS

Materials. Na$_2$SeO$_3$, vitamin C, β-thujaplicin, propidium iodide, and 6-coumarin were provided by Sigma-Aldrich. Fetal bovine serum (FBS) and Dulbecco's modified Eagle's medium (DMEM) were purchased from Gibco. LysoTracker and thiazolyl blue tetrazolium bromide (MTT) were from Sigma-Aldrich. Phosphorylated p53 (p-p53), phosphorylated AKT (p-AKT), and β-actin antibodies were purchased from Cell Signaling Technology (CST). Madin-Darby canine kidney cells (MDCK) were obtained from American Type Culture Collection (ATCC CCL-34TM). H1N1 influenza virus was provided by Guangzhou Women and Children's Medical Center, Guangzhou Medical University. Mice were obtained from the Guangdong Medical Laboratory Animal Center (Guangdong, China). All animal procedures were performed according to the guidelines of Guangdong Medical Laboratory Animal Center.
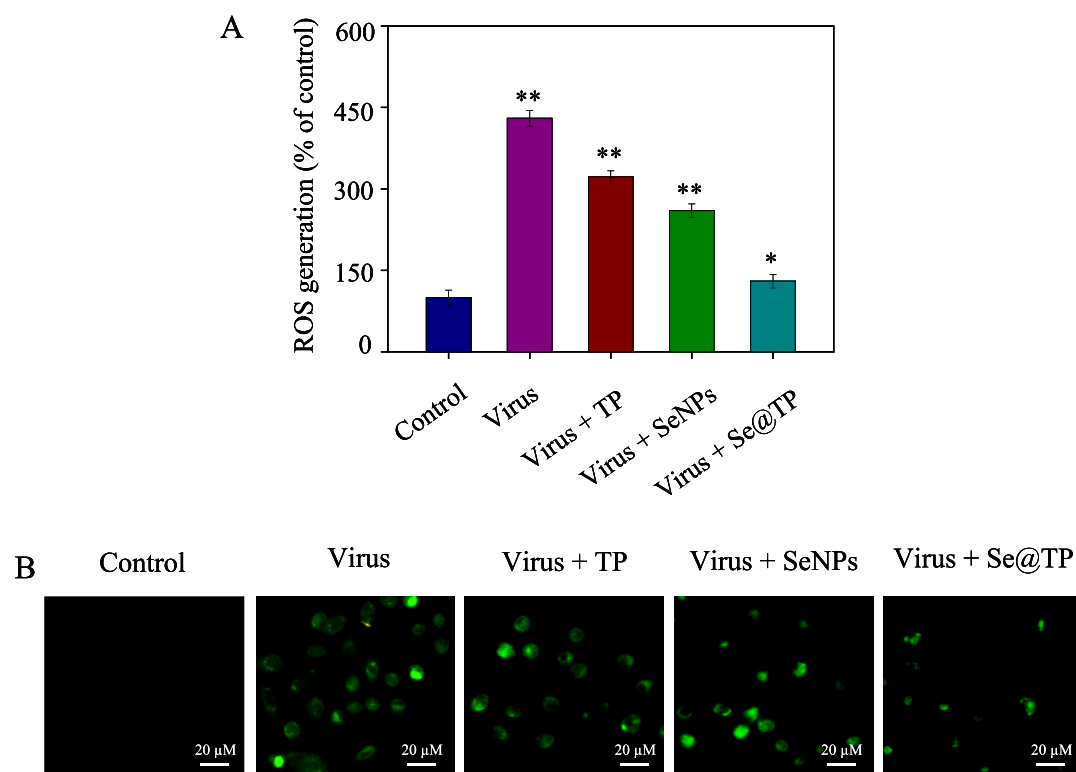
Figure 8. ROS overproduction induced by Se@TP in H1N1 infection of MDCK cells. (A) ROS levels were detected by DCF fluorescence intensity. (B) H1N1 infection of MDCK cells preincubated with 10 μM DCF for 30 min and then treated with Se@TP. Concentration of SeNPs was 1 mM and TP 10 μM. Bars with different characters are statistically different at *$p < 0.05$ or **$p < 0.01$ level.
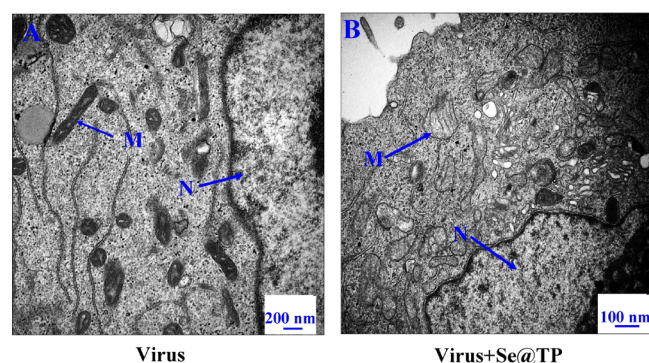

Figure 9. TEM images of thin sections of MDCK cells treated with Se@TP. (A) H1N1 virus control. (B) H1N1 virus interacted with Se@TP. (N: nucleus, M: mitochondria, and Mv: microvillus)
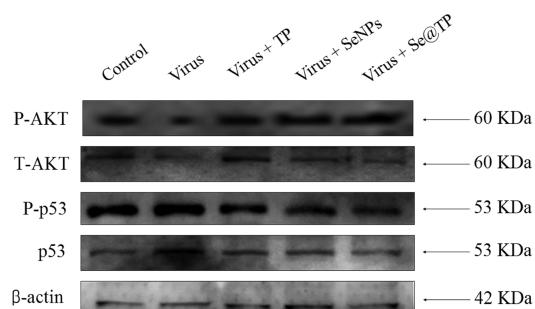

Figure 10. Intracellular apoptotic AKT and p53 signaling pathways by Se@TP in H1N1 infection of MDCK cells.

Preparation and Characterization of Se@TP. β-Thujaplicin-modified selenium nanoparticles were prepared as previously reported.[36] Stock solution of Na$_2$SeO$_3$ (0.25 mL, 0.1 M) was gradually added into 2 mL stock solution (50 mM) of vitamin C. Then, 10 μL 40 mg/mL of β-thujaplicin was added into the selenium nanoparticle solution. The excess β-thujaplicin, vitamin, and Na$_2$SeO$_3$ were removed by dialysis for overnight. Se@TP nanoparticles were sonicated and then filtered through 0.2 μm pore size. The concentration of SeNPs and TP was measured by ICP-AES. The morphology and elemental composition of Se@TP nanoparticles were characterized by transmission electron microscopy (TEM, H-7650) and EDX (EX-250 system, Horiba). Malvern Zetasizer software was used to monitor the zeta potential and size distribution of Se@TP.

Determination of Cell Viability. To detect the cell proliferation and investigate the antiviral activity of Se@TP, the cytotoxic activity of Se@TP nanoparticles was performed as previously reported.[37] First, H1N1 influenza virus was added to MDCK cells for 2 h, and then the indicated concentrations of β-thujaplicin with or without SeNPs were added to MDCK cells for 24 h. Then, MTT (20 μL/well) was added for 5 h. The formazan crystals were recorded at an absorbance of 570 nm.

Intracellular Localization of Se@TP. Endocytosis is an important pattern for the cellular uptake of extracellular nanoparticles. To investigate Se@TP nanoparticle intracellular trafficking after internalization, MDCK cells were treated with LysoTracker for 60 min as previously reported.[36] DAPI and coumarin-6-labeled Se@TP were added for various periods of time incubation. Fluorescence microscope was used to obtain and analyze the image.
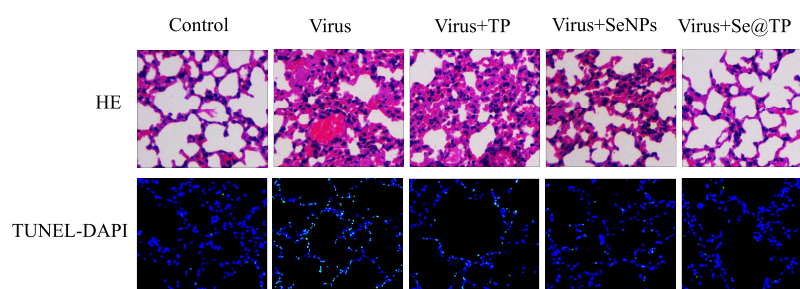
Figure 11. Histopathological analysis of Se@TP effects on the lung tissue sections of mice. *In vivo* antiviral efficiency of Se@TP. Pathologic lesions of lung tissues of HE and TUNEL-DAPI staining.
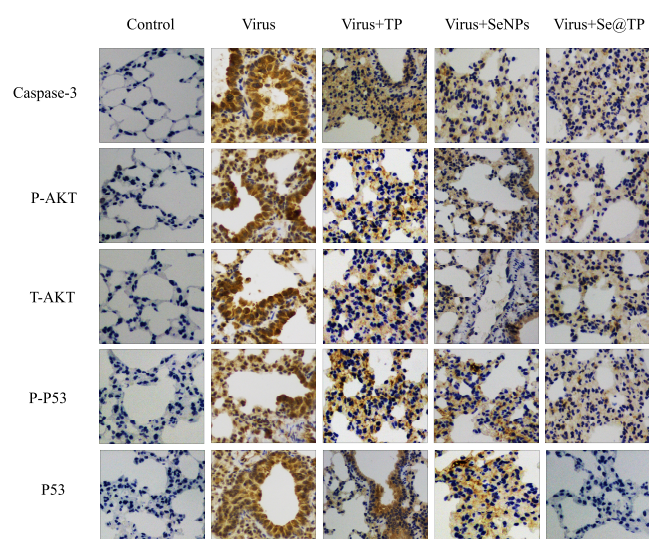

Figure 12. *In vivo* antiviral efficiency of Se@TP by immunohistochemistry of mice without infection performed as control.
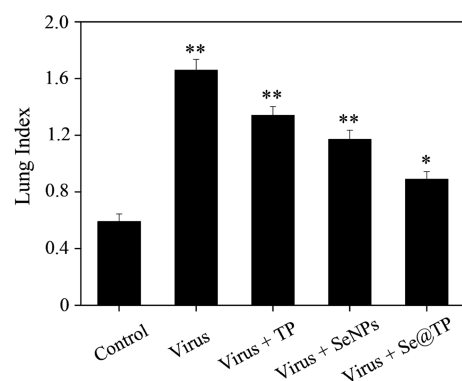

Figure 13. *In vivo* antiviral efficiency of Se@TP by lung index of mice.

Detection of Mitochondrial Membrane Potential (ΔΨm) and Annexin-V-FLUOS Staining Assay. The fluorescence intensity from JC-1 monomers was used to estimate the status of ΔΨm in MDCK cells exposed to Se@TP as previously described.[4] Plasma membrane alterations in MDCK cells treated with Se@TP were detected as previously described.[8]

Flow Cytometric Analysis and TUNEL-DAPI Costaining Assay. The effect of Se@TP on cell cycle distribution was detected through flow cytometry, and DNA fragmentation was detected using fluorescence staining by the TUNEL apoptosis kit as previously described.[37]
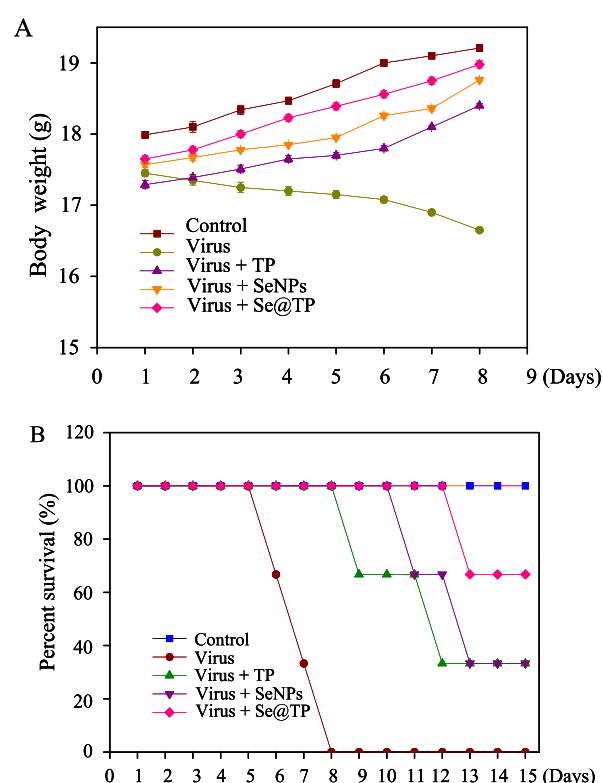

Figure 14. Body weight and survival analysis of mice influenza virus-infected BALB/c mice and treated with Se@TP. (A) Changes in body weight. (B) Survival analysis.

Caspase-3 Activity. Caspases are known to act as important mediators of apoptosis and contribute to the overall apoptotic morphology by cleavage of various cellular substrates. Activation of caspase-3 was an important event in cell apoptosis. The caspase-3 activity with the wavelengths at 380 (excitation) and 460 nm (emission) was detected as previously described.[38] DNA fragmentation was examined with fluorescence staining by the TUNEL apoptosis detection kit.[39] MDCK cells were confirmed with TUNEL for 1 h and incubated with DAPI for 15 min at 37 °C for nuclear staining.

Thin Sections of MDCK Cells and ROS Generation. To detect the target organelles by Se@TP, TEM analysis of MDCK cells was detected as previous described.[40] After incubation with H1N1 influenza virus for 2 h, MDCK cells were washed with PBS and incubated with Se@TP. Se@TP-treated MDCK cell-induced ROS accumulation was detected as previously described.[41] The overexpression of ROS could lead to DNA damage through regulation of apoptosis signaling
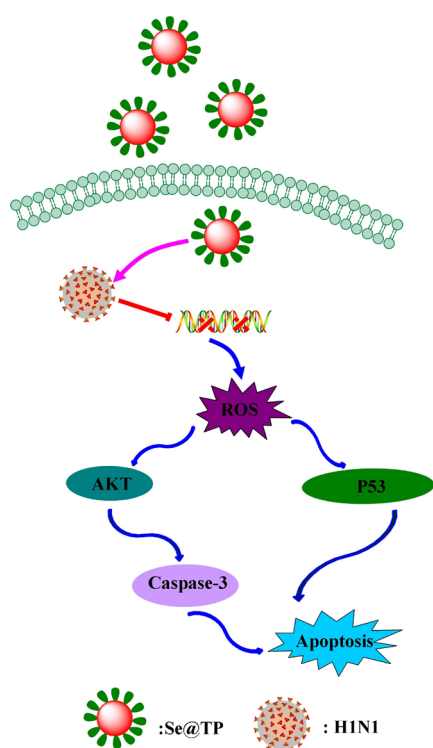
Figure 15. Apoptotic signaling pathways by Se@TP in H1N1 infection of MDCK cells. The main signaling pathway of ROS-mediated AKT and p53 signaling pathways.

pathway. The ROS generation was monitored through the fluorescence intensity (excitation 488 and emission 525 nm).

Animal Infection and Treatment. To evaluate the efficiency of Se@TP against H1N1 influenza virus *in vivo*. Thirty female BALB/c mice (aged 4−6 weeks) were randomly divided into five groups as follows: control group, H1N1 virus, virus + TP, virus + SeNPs, and virus + Se@TP. All mice were anesthetized with 10% chloral hydrate at a dose of 3 μL/g. Then, the control group was treated with 20 μL physiological saline by nasal dripping while the other four groups were treated with 20 μL H1N1 virus by nasal dripping as well. Twenty four hours later, TP, SeNPs, and Se@TP were administered to the anesthetized mice, respectively, via intranasal absorption every 24 h thereafter for a total of three times. The lungs were extracted, affused with physiological saline, and fixed in paraformaldehyde before hematoxylin and eosin (HE) staining, TUNEL test, and immunohistochemistry staining. All mice experiments were approved and guided by the Ethics Committee of Guangzhou Medical University.

Statistical Analysis. All the data are presented as mean ± SD. One-way analysis of variance (ANOVA) was used in multiple group comparisons. Difference with $P < 0.05$ (*) or $P < 0.01$ (**) was considered statistically significant.

■ AUTHOR INFORMATION

Corresponding Authors

Bing Zhu − *Center Laboratory, Guangzhou Women and Children's Medical Center, Guangzhou Medical University, Guangzhou 510120, Guangdong, People's Republic of China;* ◉ orcid.org/0000-0001-7695-6082; Phone: +86 20-81330740; Email: zhubing@gzhmu.edu.cn; Fax: +86 20 81885978

Yinghua Li − *Center Laboratory, Guangzhou Women and Children's Medical Center, Guangzhou Medical University, Guangzhou 510120, Guangdong, People's Republic of China;* ◉ orcid.org/0000-0002-6271-8283; Email: liyinghua@gzhmu.edu.cn

Authors

Changbing Wang − *Center Laboratory, Guangzhou Women and Children's Medical Center, Guangzhou Medical University, Guangzhou 510120, Guangdong, People's Republic of China*

Haiyang Chen − *Center Laboratory, Guangzhou Women and Children's Medical Center, Guangzhou Medical University, Guangzhou 510120, Guangdong, People's Republic of China*

Danyang Chen − *Center Laboratory, Guangzhou Women and Children's Medical Center, Guangzhou Medical University, Guangzhou 510120, Guangdong, People's Republic of China*

Mingqi Zhao − *Center Laboratory, Guangzhou Women and Children's Medical Center, Guangzhou Medical University, Guangzhou 510120, Guangdong, People's Republic of China*

Zhengfang Lin − *Center Laboratory, Guangzhou Women and Children's Medical Center, Guangzhou Medical University, Guangzhou 510120, Guangdong, People's Republic of China*

Min Guo − *Center Laboratory, Guangzhou Women and Children's Medical Center, Guangzhou Medical University, Guangzhou 510120, Guangdong, People's Republic of China*

Tiantian Xu − *Center Laboratory, Guangzhou Women and Children's Medical Center, Guangzhou Medical University, Guangzhou 510120, Guangdong, People's Republic of China*

Yi Chen − *Center Laboratory, Guangzhou Women and Children's Medical Center, Guangzhou Medical University, Guangzhou 510120, Guangdong, People's Republic of China*

Liang Hua − *Center Laboratory, Guangzhou Women and Children's Medical Center, Guangzhou Medical University, Guangzhou 510120, Guangdong, People's Republic of China*

Tao Lin − *Center Laboratory, Guangzhou Women and Children's Medical Center, Guangzhou Medical University, Guangzhou 510120, Guangdong, People's Republic of China*

Ying Tang − *Center Laboratory, Guangzhou Women and Children's Medical Center, Guangzhou Medical University, Guangzhou 510120, Guangdong, People's Republic of China*

Complete contact information is available at:
https://pubs.acs.org/10.1021/acsomega.0c04624

Author Contributions

C.W., H.C., and D.C. designed the study, analyzed the experimental data, and drafted the manuscript. M.Z. and Z.L. carried out the experiments. M.G. and T.X. participated in its design. Y.C., L.H., T.L., and Y.T. analyzed the data and drafted the manuscript. B.Z. and Y.L. refined the manuscript and coordination. All authors read and approved the final manuscript.

Notes

The authors declare no competing financial interest.

■ ACKNOWLEDGMENTS

and the Open Project of Guangdong Key Laboratory of Marine Materia Medica (LMM2020-7).

■ REFERENCES

(1) Dey, P.; Bergmann, T.; Cuellar-Camacho, J. L.; Ehrmann, S.; Chowdhury, M. S.; Zhang, M.; Dahmani, I.; Haag, R.; Azab, W. Multivalent Flexible Nanogels Exhibit Broad-Spectrum Antiviral Activity by Blocking Virus Entry. *ACS Nano* **2018**, *12*, 6429−6442.

(2) Wang, C.-Z.; Han, H.-H.; Tang, X.-Y.; Zhou, D.-M.; Wu, C.; Chen, G.-R.; He, X.-P.; Tian, H. Sialylglycan-Assembled Supra-Dots for Ratiometric Probing and Blocking of Human-Infecting Influenza Viruses. *ACS Appl. Mater. Interfaces* **2017**, *9*, 25164−25170.

(3) Yang, M.; Sunderland, K.; Mao, C. Virus-Derived Peptides for Clinical Applications. *Chem. Rev.* **2017**, *117*, 10377−10402.

(4) Li, Y.; Lin, Z.; Zhao, M.; Xu, T.; Wang, C.; Hua, L.; Wang, H.; Xia, H.; Zhu, B. Silver Nanoparticle Based Codelivery of Oseltamivir to Inhibit the Activity of the H1N1 Influenza Virus through ROS-Mediated Signaling Pathways. *ACS Appl. Mater. Interfaces* **2016**, *8*, 24385−24393.

(5) Jung, J. H.; Park, B. H.; Oh, S. J.; Choi, G.; Seo, T. S. Integration of reverse transcriptase loop-mediated isothermal amplification with an immunochromatographic strip on a centrifugal microdevice for influenza A virus identification. *Lab Chip* **2015**, *15*, 718−725.

(6) Londrigan, S. L.; Short, K. R.; Ma, J.; Gillespie, L.; Rockman, S. P.; Brooks, A. G.; Reading, P. C. Infection of Mouse Macrophages by Seasonal Influenza Viruses Can Be Restricted at the Level of Virus Entry and at a Late Stage in the Virus Life Cycle. *J. Virol.* **2015**, *89*, 12319−12329.

(7) Loveday, E. K.; Diederich, S.; Pasick, J.; Jean, F. Human microRNA-24 modulates highly pathogenic avian-origin H5N1 influenza A virus infection in A549 cells by targeting secretory pathway furin. *J Gen Virol.* **2015**, *96*, 30−39.

(8) Li, Y.; Lin, Z.; Zhao, M.; Guo, M.; Xu, T.; Wang, C.; Xia, H.; Zhu, B. Reversal of H1N1 influenza virus-induced apoptosis by silver nanoparticles functionalized with amantadine. *RSC Adv.* **2016**, *6*, 89679−89686.

(9) Liu, Y.; Zhang, L.; Wei, W.; Zhao, H.; Zhou, Z.; Zhang, Y.; Liu, S. Colorimetric detection of influenza A virus using antibody-functionalized gold nanoparticles. *Analyst* **2015**, *140*, 3989−3995.

(10) Hai, W.; Goda, T.; Takeuchi, H.; Yamaoka, S.; Horiguchi, Y.; Matsumoto, A.; Miyahara, Y. Specific Recognition of Human Influenza Virus with PEDOT Bearing Sialic Acid-Terminated Trisaccharides. *ACS Appl. Mater. Interfaces* **2017**, *9*, 14162−14170.

(11) Lin, Z.; Li, Y.; Guo, M.; Xu, T.; Wang, C.; Zhao, M.; Wang, H.; Chen, T.; Zhu, B. The inhibition of H1N1 influenza virus-induced apoptosis by silver nanoparticles functionalized with zanamivir. *RSC Adv.* **2017**, *7*, 742−750.

(12) Kristensen, A. B.; Lay, W. N.; Ana-Sosa-Batiz, F.; Vanderven, H. A.; Madhavi, V.; Laurie, K. L.; Carolan, L.; Wines, B. D.; Hogarth, M.; Wheatley, A. K.; Kent, S. J. Antibody Responses with Fc-Mediated Functions after Vaccination of HIV-Infected Subjects with Trivalent Influenza Vaccine. *J. Virol.* **2016**, *90*, 5724−5734.

(13) Li, M.-k.; Liu, Y.-y.; Wei, F.; Shen, M.-x.; Zhong, Y.; Li, S.; Chen, L.-j.; Ma, N.; Liu, B.-y.; Mao, Y.-d.; Li, N.; Hou, W.; Xiong, H.-r.; Yang, Z.-q. Antiviral activity of arbidol hydrochloride against herpes simplex virus I in vitro and in vivo. *Int. J. Antimicrob. Agents* **2018**, *51*, 98−106.

(14) Surov, A. O.; Manin, A. N.; Churakov, A. V.; Perlovich, G. L. New Solid Forms of the Antiviral Drug Arbidol: Crystal Structures, Thermodynamic Stability, and Solubility. *Mol. Pharmaceutics* **2015**, *12*, 4154−4165.

(15) Zhao, J.; Matsunaga, Y.; Fujita, K.; Sakai, K. Signal transduction and metabolic flux of beta-thujaplicin and monoterpene biosynthesis in elicited *Cupressus lusitanica* cell cultures. *Metab. Eng.* **2006**, *8*, 14−29.

(16) Fotopoulou, T.; Ćirić, A.; Kritsi, E.; Calhelha, R. C.; Ferreira, I. C. F. R.; Soković, M.; Zoumpoulakis, P.; Koufaki, M. Antimicrobial/Antibiofilm Activity and Cytotoxic Studies of β-Thujaplicin Derivatives. *Arch. Pharm.* **2016**, *349*, 698−709.

(17) Wang, Y.; Ding, Y.; Yang, C.; Li, R.; Du, Q.; Hao, Y.; Li, Z.; Jiang, H.; Zhao, J.; Chen, Q.; Yang, Z.; He, Z. Inhibition of the infectivity and inflammatory response of influenza virus by Arbidol hydrochloride *in vitro* and *in vivo* (mice and ferret). *Biomed. Pharmacother.* **2017**, *91*, 393−401.

(18) Kadam, R. U.; Wilson, I. A. Structural basis of influenza virus fusion inhibition by the antiviral drug Arbidol. *Proc Natl Acad Sci.* **2017**, *114*, 206−214.

(19) Damiani, G.; Eggenhöffner, R.; Pigatto, P. D. M.; Bragazzi, N. L. Nanotechnology meets atopic dermatitis: Current solutions, challenges and future prospects. Insights and implications from a systematic review of the literature. *Bioact Mater.* **2019**, *4*, 380−386.

(20) Russo, T.; Gloria, A.; De Santis, R.; D'Amora, U.; Balato, G.; Vollaro, A.; Oliviero, O.; Improta, G.; Triassi, M.; Ambrosio, L. Preliminary focus on the mechanical and antibacterial activity of a PMMA-based bone cement loaded with gold nanoparticles. *Bioact Mater.* **2017**, *2*, 156−161.

(21) Liu, W.; Li, X.; Wong, Y. S.; Zheng, W.; Zhang, Y.; Cao, W.; Chen, T. Selenium nanoparticles as a carrier of 5-fluorouracil to achieve anticancer synergism. *ACS Nano* **2012**, *6*, 6578−6591.

(22) Li, Y.; Lin, Z.; Xu, T.; Wang, C.; Zhao, M.; Xiao, M.; Wang, H.; Deng, N.; Zhu, B. Delivery of VP1 siRNA to inhibit the EV71 virus using functionalized silver nanoparticles through ROS-mediated signaling pathways. *RSC Adv.* **2017**, *7*, 1453−1463.

(23) Gustafsson, S.; Mihranyan, A. Strategies for Tailoring the Pore-Size Distribution of Virus Retention Filter Papers. *ACS Appl. Mater. Interfaces* **2016**, *8*, 13759−13767.

(24) Tao, W.; Hurst, B. L.; Shakya, A. K.; Uddin, M. J.; Ingrole, R. S. J.; Hernandez-Sanabria, M.; Arya, R. P.; Bimler, L.; Paust, S.; Tarbet, E. B.; Gill, H. S. Consensus M2e peptide conjugated to gold nanoparticles confers protection against H1N1, H3N2 and H5N1 influenza A viruses. *Antiviral Res.* **2017**, *141*, 62−72.

(25) Vonnemann, J.; Sieben, C.; Wolff, C.; Ludwig, K.; Böttcher, C.; Herrmann, A.; Haag, R. Virus inhibition induced by polyvalent nanoparticles of different sizes. *Nanoscale* **2014**, *6*, 2353−2360.

(26) Wang, J.; Zhu, R.; Gao, B.; Wu, B.; Li, K.; Sun, X.; Liu, H.; Wang, S. The enhanced immune response of hepatitis B virus DNA vaccine using SiO$_2$@LDH nanoparticles as an adjuvant. *Biomaterials* **2014**, *35*, 466−478.

(27) Shen, L.; Zhou, J.; Wang, Y.; Kang, N.; Ke, X.; Bi, S.; Ren, L. Efficient Encapsulation of Fe$_3$O$_4$ Nanoparticles into Genetically Engineered Hepatitis B Core Virus-Like Particles Through a Specific Interaction for Potential Bioapplications. *Small* **2015**, *11*, 1190−1196.

(28) Zhang, R.; Lin, Z.; Lui, V. C. H.; Wong, K. K. Y.; Tam, P. K. H.; Lee, P.; Lok, C. N.; Lamb, J. R.; Chen, Y.; Xia, H. Silver nanoparticle treatment ameliorates biliary atresia syndrome in rhesus rotavirus inoculated mice. *Nanomedicine* **2017**, *13*, 1041−1050.

(29) Stevanović, M.; Filipović, N.; Djurdjević, J.; Lukić, M.; Milenković, M.; Boccaccini, A. 45S5Bioglass (R)-based scaffolds coated with selenium nanoparticles or with poly(lactide-co-glycolide)/selenium particles: Processing, evaluation and antibacterial activity. *Colloids Surf., B* **2015**, *132*, 208−215.

(30) Huang, Y.; Luo, Y.; Zheng, W.; Chen, T. Rational Design of Cancer-Targeted BSA Protein Nanoparticles as Radiosensitizer to Overcome Cancer Radioresistance. *ACS Appl. Mater. Interfaces* **2014**, 19217−19228.

(31) Jiang, W.; Fu, Y.; Yang, F.; Yang, Y.; Liu, T.; Zheng, W.; Zeng, L.; Chen, T. *Gracilaria Iemaneiformis* Polysaccharide as Integrin-Targeting Surface Decorator of Selenium Nanoparticles to Achieve Enhanced Anticancer Efficacy. *ACS Appl. Mater. Interfaces* **2014**, *6*, 13738−13748.

(32) Wang, L.; Li, C.; Huang, Q.; Fu, X. Biofunctionalization of selenium nanoparticles with a polysaccharide from *Rosa roxburghii* fruit and their protective effect against H_2O_2-induced apoptosis in INS-1 cells. *Food Funct.* **2019**, *10*, 539−553.

(33) Cheng, Z.; Zhi, X.; Sun, G.; Guo, W.; Huang, Y.; Sun, W.; Tian, X.; Zhao, F.; Hu, K. Sodium selenite suppresses hepatitis B virus transcription and replication in human hepatoma cell lines. *J Med Virol.* **2016**, *88*, 653−663.

(34) Men, X. Y.; Xu, W. G.; Zhu, X.; Ma, W. C. Extraction, selenium-nanoparticle preparation and anti-virus bioactivity determination of polysaccharides from Caulerpa taxifolia. *Zhong Yao Cai.* **2009**, *32*, 1891−1894.

(35) Ramya, S.; Shanmugasundaram, T.; Balagurunathan, R. Biomedical potential of actinobacterially synthesized selenium nanoparticles with special reference to anti-biofilm, anti-oxidant, wound healing, cytotoxic and anti-viral activities. *J. Trace Elem. Med. Biol.* **2015**, *32*, 30−39.

(36) Li, Y.; Lin, Z.; Gong, G.; Guo, M.; Xu, T.; Wang, C.; Zhao, M.; Xia, Y.; Tang, Y.; Zhong, J.; Chen, Y.; Hua, L.; Huang, Y.; Zeng, F.; Zhu, B. Inhibition of H1N1 influenza virus-induced apoptosis by selenium nanoparticles functionalized with arbidol through ROS-mediated signaling pathways. *J.Mater. Chem. B.* **2019**, *7*, 4252−4262.

(37) Li, Y.; Lin, Z.; Zhao, M.; Xu, T.; Wang, C.; Xia, H.; Wang, H.; Zhu, B. Multifunctional selenium nanoparticles as carriers of HSP70 siRNA to induce apoptosis of HepG2 cells. *Int. J. Nanomed.* **2016**, *Volume 11*, 3065−3076.

(38) Li, Y.; Lin, Z.; Guo, M.; Zhao, M.; Xia, Y.; Wang, C.; Xu, T.; Zhu, B. Inhibition of H1N1 influenza virus-induced apoptosis by functionalized selenium nanoparticles with amantadine through ROS-mediated AKT signaling pathways. *Int. J. Nanomed.* **2018**, *Volume 13*, 2005−2016.

(39) Li, Y.; Li, X.; Zheng, W.; Fan, C.; Zhang, Y.; Chen, T. Functionalized selenium nanoparticles with nephroprotective activity, the important roles of ROS-mediated signaling pathways. *J. Mater. Chem. B* **2013**, *1*, 6365−6372.

(40) Lin, Z.; Li, Y.; Gong, G.; Xia, Y.; Wang, C.; Chen, Y.; Hua, L.; Zhong, J.; Tang, Y.; Liu, X.; Zhu, B. Restriction of H1N1 influenza virus infection by selenium nanoparticles loaded with ribavirin via resisting caspase-3 apoptotic pathway. *Int. J. Nanomed.* **2018**, *Volume 13*, 5787−5797.

(41) Guo, M.; Li, Y.; Lin, Z.; Zhao, M.; Xiao, M.; Wang, C.; Xu, T.; Xia, Y.; Zhu, B. Surface decoration of selenium nanoparticles with curcumin induced HepG2 cell apoptosis through ROS mediated p53 and AKT signaling pathways. *RSC Adv.* **2017**, *7*, 52456−52464.